Intramolecular Coupling of η^2-Iminoacyls on Zirconium Bis(aryloxides) and Calix[4]arenes: Revised Mechanism by DFT Calculations and Car−Parrinello Molecular Dynamics Simulations

Filippo De Angelis,*,† Antonio Sgamellotti,† Nazzareno Re,‡ and Simona Fantacci*,†

Istituto di Scienze e Tecnologie Molecolari (ISTM-CNR), Dipartimento di Chimica, Università di Perugia, Via Elce di Sotto 8, I-06123 Perugia, Italy, and Facoltà di Farmacia, Università G. D'Annunzio, I-66100 Chieti, Italy

Received October 29, 2004

The intramolecular coupling of the two iminoacyl units in the bis(η^2-iminoacyl) complexes [calix[4](OMe)$_2$(O)$_2$−Zr(η^2-MeCNBu^t)$_2$] and [(2,6-Bu$^t_2$C$_6$H$_3$O)$_2$−Zr(η^2-MeCNPh)$_2$] to generate the corresponding enediamido species has been investigated by means of both static and dynamic density functional calculations. For both systems we have characterized the stationary points of the potential energy surfaces for the coupling reaction and evaluated the overall energy profile. Car−Parrinello molecular dynamics simulations have been performed to gain insight into the detailed mechanistic features of the iminoacyl coupling and surprisingly show that this reaction occurs through an asynchronous reaction mechanism in which a decoordinated iminoacyl attacks the residual coordinated iminoacyl C−N double bond. A transition state search, performed without any symmetry constraint, led to structures consistent with the proposed mechanism 23.8 and 21.2 kcal mol^{-1} above the starting bis(η^2-iminoacyl) reagents, in good agreement with experimental activation enthalpies. On the basis of the proposed reaction mechanism we are also able to reproduce the activation energy of the coupling reaction with electron-withdrawing substituents on the iminoacyl moiety. Inspection of the electronic structure changes along the proposed reaction pathway suggests that the iminoacyl coupling process can be described as an intramolecular attack of the decoordinated iminoacyl carbon lone-pair at the coordinated iminoacyl π^* orbital, thus reconciling the iminoacyl coupling reaction mechanism with the generally accepted pattern of acyl and iminoacyl reactivity.

Introduction

The migratory insertion of carbon monoxide and isocyanides into metal−alkyl bonds, leading to the formation of new carbon−carbon and carbon−nitrogen bonds, has attracted widespread interest from both experimental[1−24] and theoretical points of view.[24−34] The migratory insertion of isocyanides into metal−alkyl bonds has been observed for most of the early d-block metals and leads to the formation of η^2-iminoacyl functionalities,[1,6] analogously to the carbonyl insertions which lead to η^2-acyl groups.[3,4,5,7] These reactions proceed via metal-assisted carbon−carbon bond formation and lead to a variety of carbon−metal-bonded products.

* To whom correspondence should be addressed. E-mail: filippo@thch.unipg.it (F.D.A.); simona@thch.unipg.it (S.F.).
† ISTM-Perugia.
‡ Università G. D'Annunzio.

(1) Durfee, L. D.; Rothwell, I. P. *Chem. Rev*. **1988**, *88*, 1059.
(2) Calderazzo, F. *Angew. Chem., Int. Ed. Engl.* **1977**, *16*, 299.
(3) Kulhmann, E. J.; Alexander, J. J. *Coord. Chem. Rev*. **1980**, *33*, 195.
(4) Wojcicki, A., *Adv. Organomet. Chem.* **1973**, *11*, 97.
(5) Foold, T. C. In *Topics in Stereochemistry*; Geoffroy, G. L., Ed.; Wiley: New York, 1981; Vol. 12, p 83.
(6) Alexander, J. J. In *The Chemistry of the Metal−Carbon Bond*; Hartley, F. R., Ed.; Wiley: New York, 1985; Vol. 2.
(7) Wax, M. J.; Bergman, R. G. *J. Am. Chem. Soc.* **1981**, *103*, 7028.
(8) Sigleton, E. *Adv. Organomet. Chem.* **1983**, *22*, 267.
(9) Collins, T. J.; Roper, W. R. *J. Chem. Soc., Chem. Commun.* **1976**, 1946.
(10) Facchinetti, G.; Floriani, C. *J. Organomet. Chem.* **1974**, *71*, C5.
(11) Facchinetti, G.; Fochi, G.; Floriani, C. *J. Chem. Soc., Dalton Trans.* **1977**, 1946.
(12) Erker, G. *Acc. Chem. Res.* **1984**, *17*, 103.
(13) Erker, G.; Rosenfeldt, F. *J. Organomet. Chem.* **1982**, *224*, 29−42.
(14) Moloy, K. G.; Fagan, P. J.; Manriquez, J. M.; Marks, T. J. *J. Am. Chem. Soc.* **1986**, *108*, 56.
(15) Becker, T. M.; Alexander, J. J.; Krause Bauer, J. A.; Nauss, J. L.; Wireko, F. C. *Organometallics* **1999**, *18*, 5594.
(16) Chamberlain, R. L.; Durfee, L. D.; Fanwick, P. E.; Kobriger, R.; Latesky, S. L.; McMullen, A. K.; Rothwell, I. P.; Folting, K.; Huffman, J. C.; Streib, W. E.; Wang, R. *J. Am. Chem. Soc.* **1987**, *109*, 390.
(17) Latesky, S. L.; McMullen, A. K.; Niccolai, G. P.; Rothwell, I. P.; Huffman, J. C. *Organometallics* **1985**, *4*, 1896.
(18) Durfee, L. D.; McMullen, A. K.; Rothwell, I. P. *J. Am. Chem. Soc.* **1988**, *110,* 1463.
(19) Chamberlain, R. L.; Durfee, L. D.; Fanwick, P. E.; Kobriger, R.; Latesky, S. L.; McMullen, A. K.; Steffey, B. D.; Rothwell, I. P.; Folting, K.; Huffman, J. C. *J. Am. Chem. Soc.* **1987**, *109*, 6068.
(20) Scott, M. J.; Lippard, S. J. *Organometallics* **1997**, *16*, 5857.
(21) Berg, F. J.; Petersen, J. L. *Organometallics* **1991**, *10*, 1599.
(22) Ong, T.-G.; Wood, D.; Yap, G. P. A.; Richeson, D. S. *Organometallics* **2002**, *21*, 1.
(23) Giannini, L.; Caselli, A.; Solari, E.; Floriani, C.; Chiesi-Villa, A.; Rizzoli, C.; Re, N.; Sgamellotti, A. *J. Am. Chem. Soc.* **1997**, *119*, 9709.
(24) Martins, A. M.; Ascenso, J. R.; de Azevedo, C. G.; Dias, A. R.; Duarte, M. T.; da Silva, J. F.; Veiros, L. F.; Rodrigues, S. S. *Organometallics* **2003**, *22*, 4218.

10.1021/om0491591 CCC: $30.25
Publication on Web 03/16/2005

Scheme 1

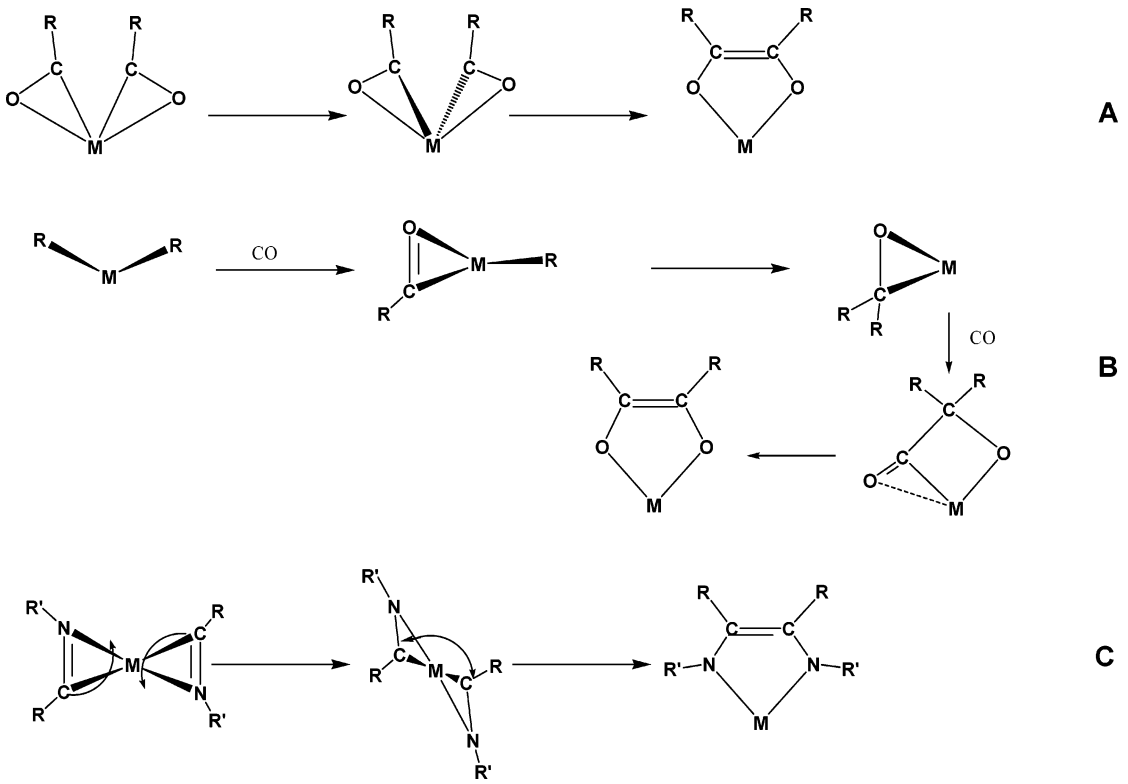

Unlike carbon monoxide, isocyanides hardly undergo deinsertion reactions but, rather, may easily give rise to multiple insertions into various metal−carbon bonds,[1,16,20−24] providing useful synthetic routes to nitrogen-containing organic compounds. Multistep isocyanide insertions have been observed for a variety of substrates, including bis(aryloxide),[1,16] tropocoronand,[20] guanidinate,[22] calix[4]arene,[23] and indenyl [24] Zr−dialkyl complexes and have been shown to generate bis(η^2-iminoacyl) functionalities. The resulting bis(η^2-iminoacyl) complexes are sufficiently stable to be isolated, and their mild thermolysis in hydrocarbon solvents induces intramolecular coupling of the two coordinated iminoacyls with formation of enediamido products.[1,17−23] The observed reactivity pattern can be included into a wider range of important carbon−carbon bond-forming reactions involving the transition-metal-assisted reductive coupling of isocyanides. Several spectroscopic studies and kinetic measurements on bis(η^2-iminoacyl) complexes of group IV metals supported by aryloxide,[17−19] cyclopentadienyl,[21] or dimethoxycalix[4]arene[23] ligands have shown the coupling reaction to be a first-order intramolecular process with activation enthalpies in the range 21−28 kcal mol^{-1}.[17−19,21,23]

This type of reactivity has been observed also upon forceful carbonylation of early-transition-metal dialkyl complexes leading to enediolate products,[35] although in this case no bis(η^2-acyl) complex has been isolated to date.

The mechanism of acyl and iminoacyl intramolecular coupling has been the subject of a few theoretical investigations.[28,29,36] For CO reductive coupling in bis(cyclopentadienyl)metal fragments two possible mechanisms have been proposed, depending on the nature of the metal. On the basis of semiempirical calculations, Tatsumi et al.[28] proposed that the reductive coupling of η^2-acyls supported by the actinide bis(cyclopentadienyl) fragment takes place from the most stable coplanar geometry via a conrotatory twisting of the two η^2-bound acyl units about their coordination axes with the metal, followed by their coupling to the enediolate product (A in Scheme 1). For this system, a bis(η^2-acyl) species, characterized by a 20-electron count at the metal, was found to be stabilized by the participation of an empty low-lying f orbital. On the other hand, for group IV metal bis(cyclopentadienyl) fragments, which cannot attain a 20-electron count, Hofmann et al.[29] proposed an alternative multistep pathway, passing through the formation of an η^2-bound ketone from the mono-η^2-acyl complex and subsequent insertion of a second CO (B in Scheme 1), which was found to be favored over pathway A by semiempirical calculations.

(25) Lauher, J. W.; Hoffmann, R. *J. Am. Chem. Soc.* **1976**, *98*, 1729.
(26) Tatsumi, K.; Nakamura, A.; Hofmann, P.; Stauffert, P.; Hoffmann, R. *J. Am. Chem. Soc.* **1985**, *107*, 4440.
(27) Hofmann, P.; Stauffert, P.; Tatsumi, K.; Nakamura, A.; Hoffmann, R. *Organometallics* **1985**, *4*, 404.
(28) Tatsumi, K.; Nakamura, A.; Hofmann, P.; Hoffmann, R.; Moloy, K. J.; Marks, T. J. *J. Am. Chem. Soc.* **1986**, *108*, 4467.
(29) Hofmann, P.; Stauffert, P.; Frede, M.; Tatsumi, K. *Chem. Ber.* **1989**, *122*, 1559.
(30) De Angelis, F.; Re, N.; Sgamellotti, A. *Organometallics* **2000**, *19*, 4904.
(31) De Angelis, F.; Sgamellotti, A.; Re, N. *J. Chem. Soc., Dalton Trans.* **2001**, 1023.
(32) Fantacci, S.; De Angelis, F.; Sgamellotti, A.; Re, N. *Organometallics* **2001**, *20*, 4031.
(33) Fantacci, S.; De Angelis, F.; Sgamellotti, A.; Re, N. *Organometallics* **2002**, *21*, 4090.
(34) De Angelis, F.; Fantacci, S.; Sgamellotti, A.; Re, N. *Theor. Chem. Acc.* **2003**, *110*, 196.
(35) Manriquez, J. M.; McAlister, D. R.; Sanner, R. D.; Bercaw, J. E. *J. Am. Chem. Soc.* **1978**, *100*, 2716.
(36) Hardesty, J. H.; Albright, T. A.; Kahlal, S. *Organometallics* **2000**, *19*, 4159.

The situation is different for iminoacyls coupling in group IV metal diaryloxide systems, for which Durfee et al.[18] originally proposed that the intramolecular reductive coupling involves a disrotatory motion of the two C−X bond vectors (C in Scheme 1); this proposal was based on the isolation and X-ray characterization of several bis(η^2-iminoacyls) all showing a head-to-tail arrangement of the two coordinated iminoacyl units[16] (C in Scheme 1). Recently, the coupling of both bis(η^2-acyl) and bis(η^2-iminoacyl) functionalities on the Zr-$(OH)_2$ fragment has been investigated by means of density functional theory (DFT) calculations by Hardesty et al.[36] For this simplified metal fragment the authors essentially confirmed the disrotatory mechanism proposed by Durfee et al. for both bis(η^2-acyl) and bis(η^2-iminoacyl) species, finding a transition state of C_2 symmetry which leads to the coupled product.

In the present study we propose an alternative mechanism for the bis(η^2-iminoacyl) coupling on diaryloxide and calix[4]arene Zr complexes, combining "static" and dynamic Car−Parrinello DFT calculations. We consider the experimentally characterized bis(η^2-iminoacyl) [*p*-Bu^t-calix[4](OMe)$_2$(O)$_2$−Zr(η^2-MeCNBu^t)$_2$] and [(2,6-Bu$^t_2$C$_6$H$_3$O)$_2$−Zr(η^2-MeCNC$_6$H$_5$)$_2$] complexes, for which kinetic parameters are available.[18,23] Moreover, to increase the generality of our study, we also consider the [(2,6-Bu$^t_2$C$_6$H$_3$O)$_2$−Zr(η^2-MeCNC$_6$H$_4$-3F)$_2$] species, obtained from [(2,6-Bu$^t_2$C$_6$H$_3$O)$_2$−Zr(η^2-MeCNC$_6$H$_5$)$_2$] by replacing a hydrogen atom by a fluorine in the para position of the phenyl rings bound to the iminoacyl nitrogens of the bis(aryloxide) complex, investigating the effect of this substitution on the activation energy of the coupling reaction. Car−Parrinello molecular dynamics simulations have been employed to study the detailed dynamic features of the iminoacyl coupling reaction while "static" DFT calculations have been performed to compute the geometries and the relative stabilities of the minima and transition states involved in the coupling reaction. This study shows that for the investigated bis(aryloxide) and calix[4]-arene Zr complexes the iminoacyl coupling occurs via an asynchronous pathway passing through a transition state in which a detached iminoacyl carbon attacks the residual coordinated iminoacyl unit. The proposed reaction mechanism is validated by comparison of computed activation parameters with experimental values.

Computational Details

We modeled the [*p*-Bu^t-calix[4](OMe)$_2$(O)$_2$] ligand by replacing the Bu^t para substituents with H atoms; it has been shown that for this class of compounds this approximation does not affect the electronic properties of the investigated systems.[37] No simplifications in the molecular structure of the [(2,6-Bu$^t_2$C$_6$H$_3$O)$_2$−Zr(η^2-MeCNC$_6$H$_5$)$_2$] bis(aryloxide) species were made.

Static DFT Calculations. All the static DFT calculations reported in this paper are based on the ADF (Amsterdam density functional) program package described elsewhere.[38] The frozen cores were 1s−4p for Zr and 1s for C and O. The molecular orbitals were expanded in an uncontracted DZ STO basis set for all atoms, with the exception of the transition-metal orbitals, for which we used a DZ STO basis set for *n*s and *n*p and a TZ STO basis set for *n*d and (*n* + 1)s. As polarization functions, one 5p, one 3d, and one 2p STO were used for Zr, O, N, and C, and H, respectively. Geometry optimizations were performed without any symmetry constraints, using the Vosko−Wilk−Nusair LDA parametrization[39] and including the Becke[40] and Perdew−Wang[41] gradient corrections to the exchange and correlation, respectively. Transition states were located using the Powell method[42] implemented in the ADF package. Due to the large size of the investigated systems, frequency calculations are not currently feasible; thus, we refer to transition states as structures that have one negative eigenvalue of the approximate Hessian matrix and the calculated energetics are therefore electronic energy differences, which do not include thermal corrections to the entropy and enthalpy. The accuracy of the employed exchange-correlation functional in determining activation parameters for insertion reactions into Zr−alkyl bonds has been checked in a previous study.[30]

Car-Parrinello Calculations. Car−Parrinello[43] (CP) molecular dynamics simulations were carried out on a slightly simplified model of the complex [calix[4](OMe)$_2$(O)$_2$−Zr(η^2-MeCNBu^t)$_2$], in which the Bu^t groups bound to the iminoacyl nitrogens were replaced by methyl groups. The parallel version[44] of the CP code implementing Vanderbilt pseudopotentials [45,46] was used. For the LDA exchange-correlation functional the Perdew−Zunger parametrization[47] has been used, while the gradient-corrected functional is taken from ref 48. Core states are projected out using pseudopotentials. For Zr, C, O, and H "ultra-soft" pseudopotentials were generated according to the scheme proposed by Vanderbilt.[46] The wave functions (density) were expanded in plane waves up to an energy cutoff of 25 (200) Ry. Periodic boundary conditions were used by placing the model molecule in a cubic box of 15.87 Å, keeping a minimum of 6.0 Å between repeated images, which is sufficiently large to avoid any coupling between periodic images. The equations of motion were integrated using a time step of 10 au (0.242 fs) with an electronic fictitious mass μ = 1000 au. Constrained CP simulations were performed by means of the SHAKE algorithm,[49] employing the slow-growth method,[50] in which the constrained parameter is slowly varied as a function of the simulation time, in such a way that the potential energy surface along the considered constraint is dynamically sampled; to maintain the system in thermal equilibrium, the temperature of the nuclei was controlled by a Nosè thermostat,[51] which creates a canonical (NVT) ensemble. To obtain a thermal distribution of vibrational modes, the temperature was gradually increased by small steps. We note that this technique has been first applied to CO migratory insertions by Margl et al.[52] A point which needs to be stressed

(37) Fantacci, S.; Sgamellotti, A.; Re, N.; Floriani, C. *J. Chem. Soc., Dalton Trans.* **2001**, 1718.

(38) (a) te Velde, G.; Bickelhaupt, F. M.; Baerends, E. J.; Fonseca Guerra, C.; van Gisbergen, S. J. A.; Snijders, J. G.; Ziegler, T. *J. Comput. Chem.* **2001**, *22*, 931. (b) Fonseca Guerra, C.; Visser, O.; Snijders, J. G.; te Velde, G.; Baerends, E. J. In *Methods and Techniques for Computational Chemistry*; Clementi, E., Corongiu, C., Eds.; STEF: Cagliari, Italy, 1995; pp 303−395.

(39) Vosko, S. H.; Wilk, L.; Nusair, M. *Can. J. Phys.* **1980**, *58*, 1200.

(40) Becke, A. D. *Phys. Rev.* **1988**, *A38*, 3098.

(41) Perdew, J. P.; Wang, Y. *Phys. Rev.* **1992**, *B45*, 13244.

(42) Powell, M. J. D. *Math. Prog.* **1977**, *12*, 241.

(43) Car, R.; Parrinello, M. *Phys. Rev. Lett.* **1985**, *55*, 2471.

(44) Giannozzi, P.; De Angelis, F.; Car, R. *J. Chem. Phys.* **2004**, 120, 5903.

(45) (a) Pasquarello, A.; Laasonen, K.; Car, R.; Lee, C.; Vanderbilt, D. *Phys. Rev. Lett.* **1992**, *69*, 1982. (b) Pasquarello, A.; Laasonen, K.; Car, R.; Lee, C.; Vanderbilt, D. *Phys. Rev. B* **1993**, *47*, 10142.

(46) Vanderbilt, D. *Phys. Rev. B* **1990**, *41*, 7892.

(47) Perdew, J. P.; Zunger, A. *Phys. Rev. B* **1981**, *23*, 5048.

(48) Perdew, J. P.; Chevary, J. A.; Vosko, S. H.; Jackson, K. A.; Pederson, M. R.; Singh, D. J.; Fiolhais, C. *Phys. Rev. B* **1992**, *46*, 6671.

(49) Ryckaert, J.-P.; Ciccotti, G.; Berendsen, H. J. C. *J. Comput. Phys.* **1977**, *23*, 327.

(50) Straatsma, T. P.; Berendsen, H. J. C.; Postma, J. P. M. *J. Chem. Phys.* **1986**, *85*, 6720.

(51) Nosè, S. *Mol. Phys.* **1984**, *52*, 255.

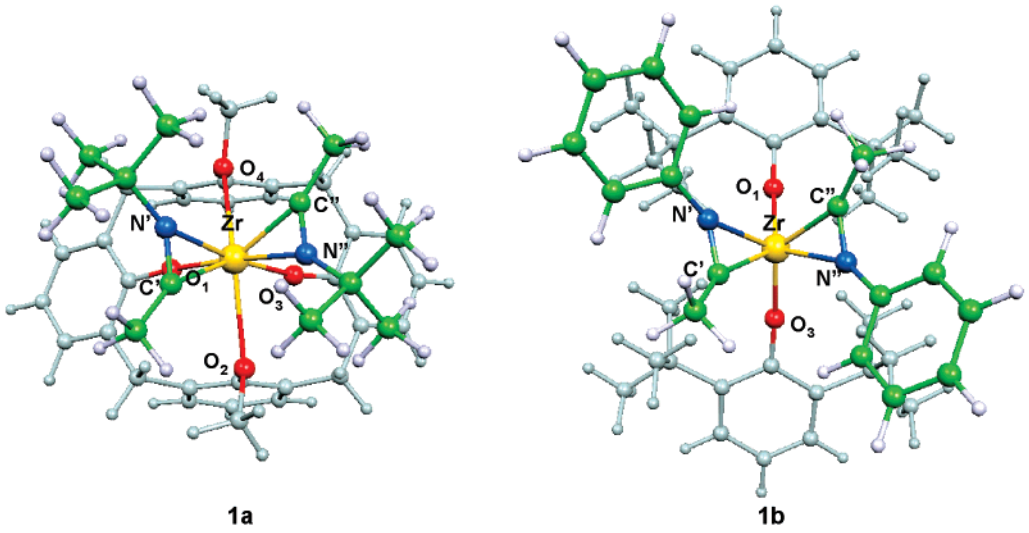

Figure 1. Optimized geometrical structures of the calix[4]arene and bis(aryloxide) bis(η^2-iminoacyl) complexes **1a**,**b**. Legend: Zr, yellow; O, red; N, light blue; C atoms bound to the iminoacyl moieties, green; H atoms and C atoms of the calix[4]arene and of the bis(aryloxide) ligands, gray.

here is that we only mean to exploit the power of CP simulations to sample the reactive potential energy surface, without performing any thermodynamical integration along the approximate reaction coordinate (RC). Such a procedure can be reasonably accurate only if the approximate RC has a high projection onto the reaction mode and would be better performed considering a constrained motion of the system along a predetermined multidimensional intrinsic reaction pathway, as recently suggested by Michalak et al.[53] The consistency of the CP and ADF programs has been checked in ref 32 by comparing the geometries of the fully optimized [calix[4](OMe)$_2$(O)$_2$−Zr(Me)$_2$] complex with the analogous [p-Bu^t-calix[4](OMe)$_2$(O)$_2$−Zr(CH$_2$Ph)$_2$ complex, for which X-ray data are available.[23]

Results and Discussion

Bis(η^2-iminoacyl) Complexes. We start our analysis by optimizing the geometry of the bis(η^2-iminoacyl) complexes [calix[4](OMe)$_2$(O)$_2$−Zr(η^2-MeCNBu^t)$_2$] (**1a**) and [(2,6-Bu$^t_2$C$_6$H$_3$O)$_2$−Zr(η^2-MeCN(C$_6$H$_5$))$_2$] (**1b**), considering both a head-to-tail and a head-to-head arrangement of the two iminoacyl units. Hereafter we refer to O_1, O_3 as the phenoxo oxygens and O_2, O_4 as the methoxy oxygens of the calix[4]arene complexes, respectively, maintaining the same labeling for the aryloxide oxygens of complex **1b**; we indicate the carbon and nitrogen atoms of the two iminoacyl units as C′, N′ and C″, N″ (see Figure 1).

Table 1. Optimized Geometrical Parameters (Distances in Å and Angles in deg) of Bis(η^2-iminoacyl) Complexes 1a,b, Compared to Available Experimental Data

	1a		1b	
param	theor	exptl[a]	theor	exptl[b]
Zr−O$_1$	2.094	2.054(4)	2.099	2.027(2)
Zr−O$_2$	2.675	2.450(5)		
Zr−O$_3$	2.095		2.125	
Zr−O$_4$	2.644			
Zr−C′	2.281	2.259(6)	2.249	2.228(3)
Zr−N′	2.296	2.249(4)	2.237	2.221(3)
C′−N′	1.278	1.271(8)	1.296	1.286(4)
Zr−C″	2.279		2.243	
Zr−N″	2.299		2.256	
C″−N″	1.278		1.296	
O$_1$−Zr−O$_3$	93.8	91.9	104.0	97.3(1)
O$_2$−Zr−O$_4$	144.3	143.8		
Zr−C′−N′	74.5	73.2	72.7	72.9(2)
Zr−C″−N″	74.6		73.8	

[a] Data from ref 23. [b] Data from ref 16.

We find the head-to-tail configuration of the two iminoacyl units to be energetically favored with respect to the head-to-head arrangement by 4.3 and 5.2 kcal mol^{-1} for complexes **1a**,**b**, respectively, in agreement with the experimentally characterized structures. The higher stability of a head-to-tail arrangement with respect to a head-to-head one is mainly related to the steric hindrance exerted by the bulky Bu^t and Ph substituents bound to the iminoacyl nitrogens, which is minimized in the former configuration. The optimized structures are in good agreement with available experimental data (see Table 1) (the structure of **1b** is compared to that of the closely related [(2,6-Bu$^t_2$C$_6$H$_3$O)$_2$−Zr(η^2-Bu^{t}CNCH$_2$Ph)$_2$] complex, for which X-ray data are available[16]). The two iminoacyl units are almost sym-

(52) Margl, P.; Ziegler, T.; Blöchl, P. E. *J. Am. Chem. Soc.* **1996**, *118*, 5412.
(53) Michalak, A.; Ziegler, T. *J. Phys. Chem. A* **2001**, *17*, 4333.
(54) Frisch, M. J.; Trucks, G. W.; Schlegel, H. B.; Scuseria, G. E.; Robb, M. A.; Cheeseman, J. R.; Montgomery, J. A., Jr.; Vreven, T.; Kudin, K. N.; Burant, J. C.; Millam, J. M.; Iyengar, S. S.; Tomasi, J.; Barone, V.; Mennucci, B.; Cossi, M.; Scalmani, G.; Rega, N.; Petersson, G. A.; Nakatsuji, H.; Hada, M.; Ehara, M.; Toyota, K.; Fukuda, R.; Hasegawa, J.; Ishida, M.; Nakajima, T.; Honda, Y.; Kitao, O.; Nakai, H.; Klene, M.; Li, X.; Knox, J. E.; Hratchian, H. P.; Cross, J. B.; Adamo, C.; Jaramillo, J.; Gomperts, R.; Stratmann, R. E.; Yazyev, O.; Austin, A. J.; Cammi, R.; Pomelli, C.; Ochterski, J. W.; Ayala, P. Y.; Morokuma, K.; Voth, G. A.; Salvador, P.; Dannenberg, J. J.; Zakrzewski, V. G.; Dapprich, S.; Daniels, A. D.; Strain, M. C.; Farkas, O.; Malick, D. K.; Rabuck, A. D.; Raghavachari, K.; Foresman, J. B.; Ortiz, J. V.; Cui, Q.; Baboul, A. G.; Clifford, S.; Cioslowski, J.; Stefanov, B. B.; Liu, G.; Liashenko, A.; Piskorz, P.; Komaromi, I.; Martin, R. L.; Fox, D. J.; Keith, T.; Al-Laham, M. A.; Peng, C. Y.; Nanayakkara, A.; Challacombe, M.; Gill, P. M. W.; Johnson, B.; Chen, W.; Wong, M. W.; Gonzalez, C.; Pople, J. A. *Gaussian 03*, revision B.04; Gaussian, Inc.: Pittsburgh, PA, 2003.
(55) Hay, P. J.; Wadt, W. R. *J. Chem. Phys.* **1985**, *82*, 270. Hay, P. J.; Wadt, W. R. *J. Chem. Phys.* **1985**, *82*, 284. Hay, P. J.; Wadt, W. R. *J. Chem. Phys.* **1985**, *82*, 299.
(56) Ditchfield, R.; Herhe, W. J.; Pople, J. A. *J. Comput. Chem.* **1971**, *54*, 724.

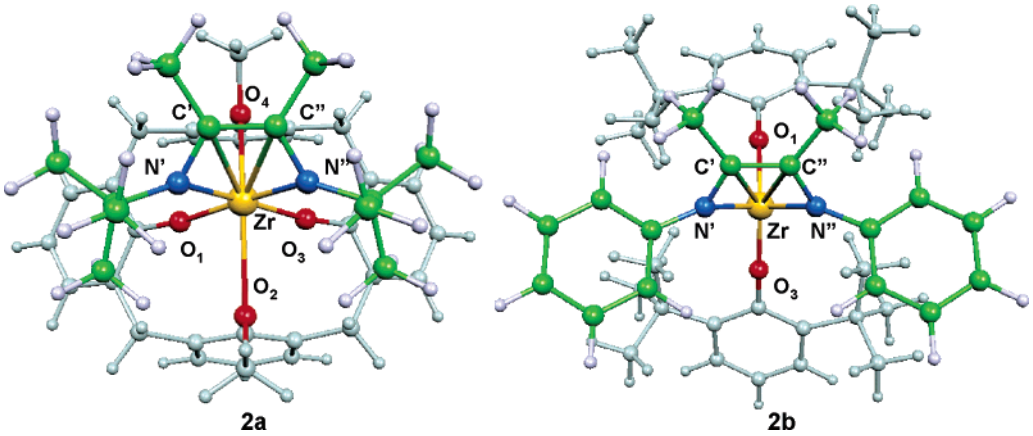

Figure 2. Optimized geometrical structures of the calix[4]arene and bis(aryloxide) enediamido complexes **2a**,**b**. The color codes are the same as in Figure 1.

metric, with double C−N bonds of 1.278 and 1.296 Å in **1a**,**b**, respectively, in excellent agreement with experimental values of 1.271(8) and 1.286(4) Å. Again in agreement with X-ray data, we compute almost comparable values for the Zr−C and Zr−N distances in the two complexes, with values of 2.280, 2.296 Å and 2.243, 2.256 Å for **1a**,**b**, respectively, to be compared to experimental values of 2.259(6), 2.249(4) Å and 2.228(3), 2.221(3) Å. We note that in complex **1a** the iminoacyl C−N bonds lie parallel to the O_2−Zr−O_4 plane, while in **1b** the C−N bonds are parallel to the O_1−Zr−O_3 plane (see Figure 1), probably as a result of the steric hindrance exerted by the methoxy groups bound to O_2 and O_4 in the bis(η^2-iminoacyl) calix[4]arene complex **1a**.

Enediamido Complexes. The products of the intramolecular coupling of the two iminoacyl units in the calix[4]arene and bis(aryloxide) complexes are the enediamido species **2a**,**b**, respectively (see Figure 2). The structures of both enediamido complexes were optimized, showing **2a**,**b** to be 16.4 and 30.7 kcal mol^{-1} below the corresponding bis(η^2-iminoacyl) complexes, respectively. The different stabilities of **2a**,**b** are probably related to the fact that in the calix[4]arene enediamido complex **2a** the metallacycle moiety is forced to lie in the plane of the phenoxo O_1 and O_3 oxygens, while in **2b** an almost tetrahedral coordination of the Zr(IV) center can be achieved. The quite high computed exothermicity is consistent with the observed irreversibility of the coupling reaction.

Main optimized geometrical parameters of complexes **2a**,**b** are reported in Table 2, together with the X-ray data available for the corresponding complexes p-Bu^t-calix[4](OMe)$_2$(O)$_2$−Zr[N(Bu^t)C(Me)=C(Me)N-(Bu^t)][23] and (OAr-2,6Bu$^t_2$)$_2$−Zr[(2,6-Me$_2$Ph)NC(Me)=C-(Me)N(2,6-Me$_2$Ph)][19] complexes. Both enediamido complexes **2a**,**b** show a folded metallacycle unit with a double C=C bond coordinated to the electron-deficient Zr(IV) center. Average Zr−C distances of 2.630 and 2.665 Å are computed in **2a**,**b**, respectively, in good agreement with the experimental value of 2.698(7) Å found for **2b**. The puckering of the metallacycle in the enediamido complexes is confirmed by the value of the ∠N′ZrN″C′ dihedral angle, which is computed to be 47.0 and 44.9° in **2a**,**b**, respectively.

An interesting feature of these enediamido complexes is that the folded metallacycle unit undergoes a dynamical ring flip, as detailed by Rothwell in refs 17 and 19, where an estimate of the free energy barrier associated with the ring flip process was provided. Notably, we computed the transition state for the ring flip in complex **2b**, which corresponds to an almost planar arrangement of the metallacycle unit, finding an energy barrier of 17.6 kcal mol^{-1}, in excellent agreement with the experimental activation free energy of 15.5(35) kcal mol^{-1} found for **2b**.[19] We note that a higher exothermicity of the iminoacyl coupling reaction (−45.4 kcal mol^{-1}) and a lower energy barrier for the enediamido ring flip process (12.2 kcal mol^{-1}) were computed for the reduced model of ref 36, probably due to the modeling of the alkoxide ligands by hydroxides and to the replacement of the bulky alkyl and aryl groups bound to the iminoacyl units by hydrogen atoms.

Table 2. Optimized Geometrical Parameters (Distances in Å and Angles in deg) of Enediamido Complexes 2a,b, Compared to Available Experimental Data

	2a		2b	
param	theor	exptl[a]	theor	exptl[b]
Zr−O_1	2.082	2.031(5)	2.010	1.950(4)
Zr−O_2	2.400	2.401(3)		
Zr−O_3	2.083	2.037(4)	2.054	2.009(4)
Zr−O_4	2.655			
Zr−C′	2.639		2.659	2.698(7)
Zr−C″	2.622		2.670	2.698(7)
Zr−N′	2.148	2.104(7)	2.099	2.061(15)
C′−N′	1.403	1.507(9)	1.403	1.439(8)
Zr−N″	2.135	2.097(7)	2.116	2.060(6)
C″−N″	1.408	1.450(15)	1.407	1.420(8)
C′−C″	1.400	1.385(13)	1.394	1.366(9)
O_1−Zr−O_3	93.5	94.5(2)	116.2	114.0(2)
O_2−Zr−O_4	145.6	146.2(1)		
Zr−N′−C′	93.2	90.3(4)	96.7	102.0(4)
Zr−N″−C″	93.6	89.5(6)	96.6	99.4(4)

[a] Data from ref 23. [b] Data from ref 19.

Dynamics Simulations. To gain insight into the reaction mechanism of the intramolecular bis(η^2-iminoacyl) coupling, we performed CP molecular dynamics simulations on the model of the bis(η^2-iminoacyl) complex **1a** (see Computational Details). With its optimized geometry as the starting point, the system was equilibrated for 1.0 ps at 350 K. Thereafter, the iminoacyl intramolecular C′−C″ distance, assumed as an approximate reaction coordinate (RC), was constrained to vary in the range 3.3−1.4 Å during a total time span of

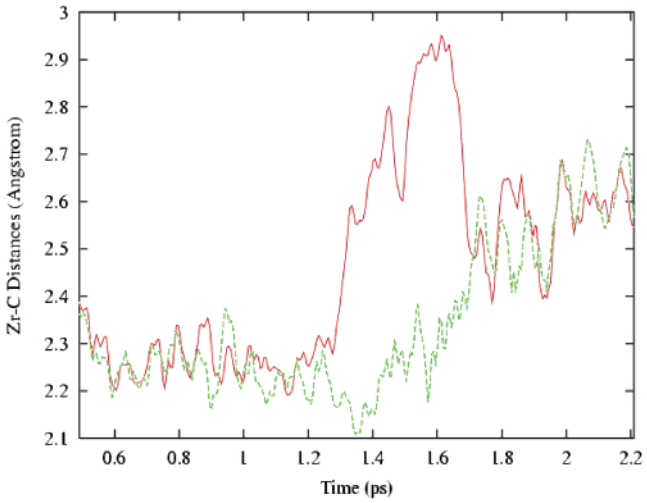

Figure 3. Evolution of the Zr−C′ (green line) and Zr−C″ (red line) distances as a function of the simulation time for the time slice 0.5−2.2 ps. Distances are given in Å and time in ps.

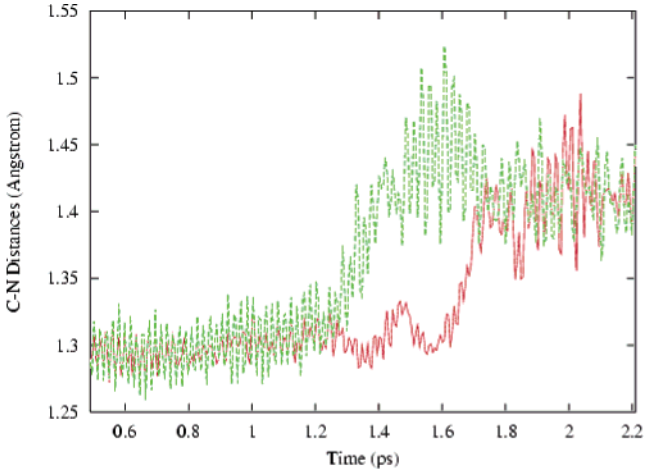

Figure 4. Evolution of the C′−N′ (green line) and C″−N″ (red line) distances as a function of the simulation time for the time slice 0.5−2.2 ps. Distances are given in Å and time in ps.

1.8 ps, allowing all the degrees of freedom corresponding to the transversal modes to follow their natural evolution. After 1.8 ps the constraint on the C′−C″ distance was removed, allowing the system to evolve naturally in time for an additional 0.4 ps. The iminoacyl C′−C″ distance represents a natural choice for the approximate RC, since its variation connects the reagent and product basins, accounting for the intramolecular formation of the new carbon−carbon bond. A movie file with the CP trajectory is available as Supporting Information.

The iminoacyl coupling reaction can be followed by studying the evolution of the Zr−C′ and Zr−C″ distances as a function of the simulation time, or approximate RC. Indeed, for a synchronous conrotatory or disrotatory process the Zr−C′ and Zr−C″ distances are expected to remain initially constant and then, after the iminoacyl coupling, to increase in a parallel fashion from their initial values of ca. 2.3 Å in the starting bis(η^2-iminoacyl) complex up to ca. 2.6 Å in the enediamido product. Figure 3 displays the time evolution of the Zr−C′ and Zr−C″ distances and surprisingly shows that the intramolecular carbon−carbon bond formation takes place via an asynchronous reaction mechanism. Indeed, after 1.3 ps (corresponding to a value of the C′−C″ distance of 1.87 Å), the Zr−C″ distance exhibits a wide oscillation up to 2.95 Å, indicating the detachment of the carbon atom of one iminoacyl unit from the metal center. On the other hand, the Zr−C′ distance keeps on oscillating around its equilibrium value in the bis(η^2-iminoacyl) reagent up to 1.6 ps (corresponding to a C′−C″ distance of 1.54 Å), and only after 1.6 ps it increases to a value close to 2.5 Å, reaching the Zr−C″ value. After ca. 2.0 ps both Zr−C distances oscillate around 2.6 Å, a value close to that of the metal-coordinated carbon−carbon bond in the enediamido product.

Further insight into the reaction mechanism can be gained by analyzing the evolution of the C′−N′ and C″−N″ distances, plotted as a function of the simulation time in Figure 4. The considered parameters are expected to increase from their initial values below 1.3 Å in the starting bis(iminoacyl) reagent up to ca. 1.4 Å in the enediamido product, reflecting the change from double to almost single C−N bonds. As can be noticed from Figure 4, the time evolution of the C′−N′ and C″−N″ distances confirms the asynchronous character of the reaction mechanism and suggests that the reactive event can be described as an intramolecular attack of the detached iminoacyl carbon to the residual coordinated iminoacyl. Indeed, while the C″−N″ distance corresponding to the decoordinated iminoacyl unit does not show significant variations up to ca. 1.6 ps, the C′−N′ distance increases from its initial value close to 1.3 to ca. 1.5 Å within 1.6 ps. After 1.7 ps both distances oscillate around ca. 1.4 Å, corresponding to their equilibrium values in the enediamido product. Interestingly, the intramolecular coupling is accompanied by a change in the coordination plane of both iminoacyl units, which rotate by about 90° around the Zr−C and Zr−N bonds within 1.3 ps, so that the decoordinated iminoacyl attack takes place with the coordinated iminoacyl unit almost lying in the O_1−Zr−O_3 plane, as opposed to the arrangement found for the starting bis(η^2-iminoacyl) **1a**, in which the two iminoacyl units were lying perpendicular to the O_1−Zr−O_3 plane.

We notice that the asynchronous reaction mechanism outlined above is not determined by the particular choice of the approximate RC, since in principle a synchronous (conrotatory or disrotatory) reaction pathway might well take place following the system evolution along the same RC. The fact that a synchronous reaction pathway is not sampled during the CP molecular dynamics simulations suggests that this pathway is higher in energy than the proposed asynchronous one (see below).

Transition States and Energetics of the Intramolecular Coupling. Extracting selected configurations from the dynamics simulations, we have been able to optimize the geometry of the transition states connecting the bis(η^2-iminoacyl) complexes **1a**,**b** to the corresponding enediamido species **2a**,**b** for the calix[4]-arene and bis(aryloxide) systems $\mathbf{TS_{1a\rightarrow 2a}}$ and $\mathbf{TS_{1b\rightarrow 2b}}$, respectively, finding the structures reported in Figure 5. It is worth noting that similar asymmetric transition state structures are computed for both the calix[4]arene and bis(aryloxide) complexes, suggesting the similarity of the reaction pathways in the two species. Notably, both $\mathbf{TS_{1a\rightarrow 2a}}$ and $\mathbf{TS_{1b\rightarrow 2b}}$ show an η^2-coordinated

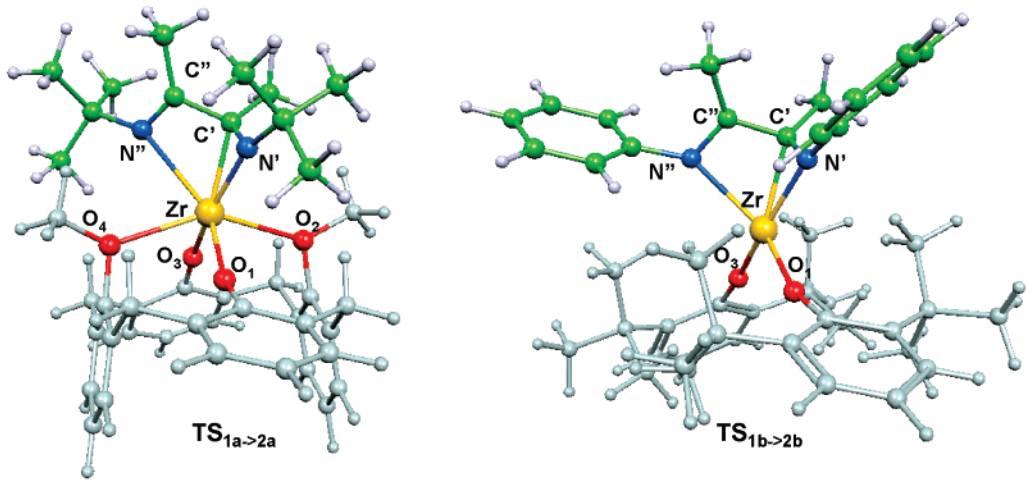

Figure 5. Optimized geometrical structures of the transition states $\mathbf{TS_{1a\rightarrow 2a}}$ and $\mathbf{TS_{1b\rightarrow 2b}}$ for the asynchronous coupling reaction pathway in the calix[4]arene and bis(aryloxide) systems. The color codes are the same as in Figure 1.

Table 3. Optimized Geometrical Parameters (Distances in Å and Angles in deg) of Transition States $\mathbf{TS_{1a\rightarrow 2a}}$, $\mathbf{TS_{1b\rightarrow 2b}}$, and $\mathbf{TS_{1c\rightarrow 2c}}$

param	$\mathbf{TS_{1a\rightarrow 2a}}$	$\mathbf{TS_{1b\rightarrow 2b}}$	$\mathbf{TS_{1c\rightarrow 2c}}$
Zr−C′	2.234	2.252	2.261
Zr−N′	2.117	2.176	2.192
C′−N′	1.438	1.444	1.446
Zr−C″	2.934	2.729	2.729
Zr−N″	2.757	2.413	2.428
C″−N″	1.296	1.322	1.326
C′−C″	1.506	1.488	1.493
C″−C′-Zr−N′	112.0	102.3	102.0

iminoacyl lying in the plane containing the phenoxo oxygens and the metal being attacked by a decoordinated iminoacyl unit, as confirmed by the values of the ∠C″−C′−Zr−N′ dihedral angles of 112.0 and 102.3° for $\mathbf{TS_{1a\rightarrow 2a}}$ and $\mathbf{TS_{1b\rightarrow 2b}}$, respectively (see Figure 5 and Table 3). This suggests that the coupling reaction may be described as an intramolecular attack of the detached iminoacyl carbon at the coordinated iminoacyl π^* orbital. This is analogous to the mechanism found in the methyl to acyl and methyl to iminoacyl migrations in the Zr−calix[4]arene fragment, which was found to be related to the spatial orientation of the acyl and iminoacyl π^* LUMO favoring such a lateral attack.[30−34]

We compute $\mathbf{TS_{1a\rightarrow 2a}}$ and $\mathbf{TS_{1b\rightarrow 2b}}$ to lie 21.2 and 23.8 kcal mol^{-1} above the corresponding bis(η^2-iminoacyl) complexes (see the energetics of the coupling reaction in Figure 6), in good agreement with the experimental activation enthalpies of 25.4(5) and 21.8(9) kcal mol^{-1} for the calix[4]arene and bis(aryloxide) species, respectively. Moreover, we optimized the transition state ($\mathbf{TS_{1c\rightarrow 2c}}$) for the coupling reaction in the bis(η^2-iminoacyl) complex [(2,6-Bu$^t_2$C$_6$H$_3$O)$_2$−Zr(η^2-MeCN(C$_6$H$_4$-3-F))$_2$] (**1c**), obtained from **1b** by substituting a hydrogen by a fluorine atom in the para positions of the phenyl substituents bound to the iminoacyl nitrogens. Optimization of the equilibrium structure of **1c** allowed us to compute an activation energy of 26.5 kcal mol^{-1} for the coupling reaction from **1c**, again in good agreement with the activation enthalpy of 27.7(10) kcal mol^{-1} measured for this system.[18]

To further support the validity of the proposed asynchronous reaction mechanism, for the reduced model of the Zr−calix[4]arene species we optimized the geometry of both the transition state corresponding to a synchronous coupling reaction and of the bis(η^2-iminoacyl) reagent imposing C_2 symmetry constraints. In this stage we used the Gaussian03 program package,[54] employing the same BPW91 exchange-correlation potential used for the ADF calculations. A LANL2DZ basis set[55] along with the corresponding pseudopotential was used for Zr, while a 6-31g* basis set[56] was used for all the other atoms. The transition state for the synchronous coupling reaction was located on the C_2 potential energy surface 40.3 kcal mol^{-1} above the starting bis(η^2-iminoacyl) reagent. The geometry of this transition state is quite similar to that reported by Hardesty et al.,[36] with a C−C distance of 1.78 Å and slightly elongated Zr−C distances (2.35 Å). The computed energy barrier is 20.1 kcal mol^{-1} higher than that computed for the asynchronous reaction pathway from **1a** (21.2 kcal mol^{-1}), thus ruling out the synchronous reaction mechanism for this system.

Electronic Structure along the Coupling Process. At this point a thorough inspection of the frontier orbitals of the calix[4]arene system and their changes along the coupling process has been performed to provide insight into the electronic factors governing the proposed reaction mechanism. In particular, since the coupling reaction occurs via an asynchronous mechanism in which an iminoacyl carbon is detached from the metal prior to its attack to the residual coordinated η^2-bound iminoacyl unit, we sought to disentangle the motion along the Zr−C″ coordinate from that occurring along the C′−C″ coordinate. To this aim, we performed a linear transit scan of the potential energy surface, assuming the Zr−C″ distance as an approximate reaction coordinate. Geometry optimizations were performed, without any symmetry constraints, starting from the optimized geometry of the bis(η^2-iminoacyl) complex **1a**, by keeping fixed the Zr− C″ distance at selected values in the range of 2.27−3.00 Å and relaxing all the other geometrical parameters.

Inspection of the electronic structure of **1a** at its equilibrium geometry reveals that the highest occupied molecular orbital (HOMO) is a bonding combination of the iminoacyl carbon and nitrogen p orbitals with the zirconium d orbitals, symmetrically delocalized on the two iminoacyl units (see Figure 7). The lowest unoc-

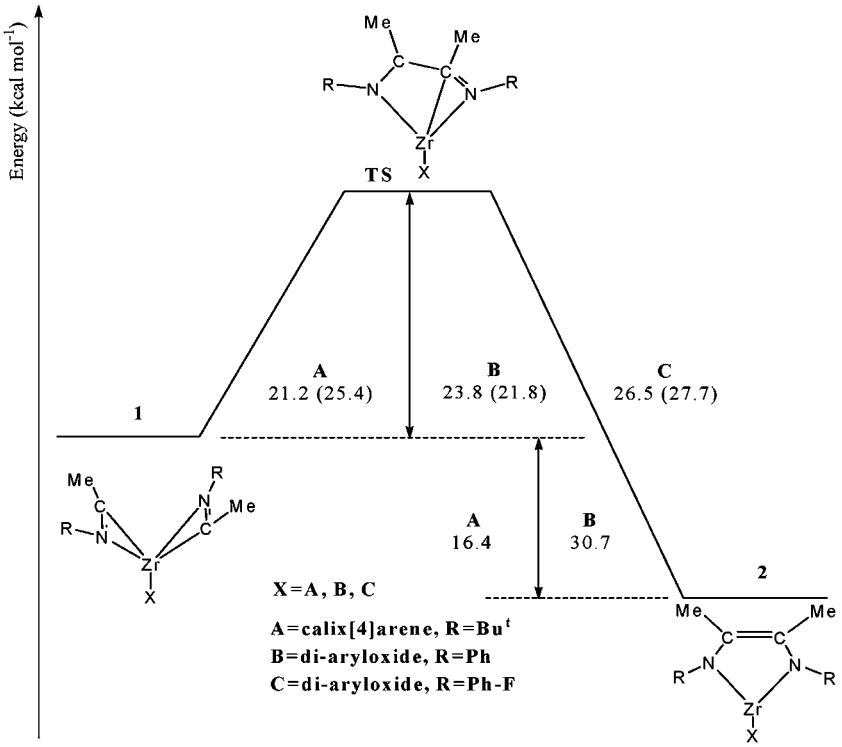

Figure 6. Computed energetics (kcal mol^{-1}) of the iminoacyl coupling reaction from the initial bis(η^2-iminoacyl) complexes **1a**−**c**, compared to available experimental data (in parentheses) from refs 23 and 18.

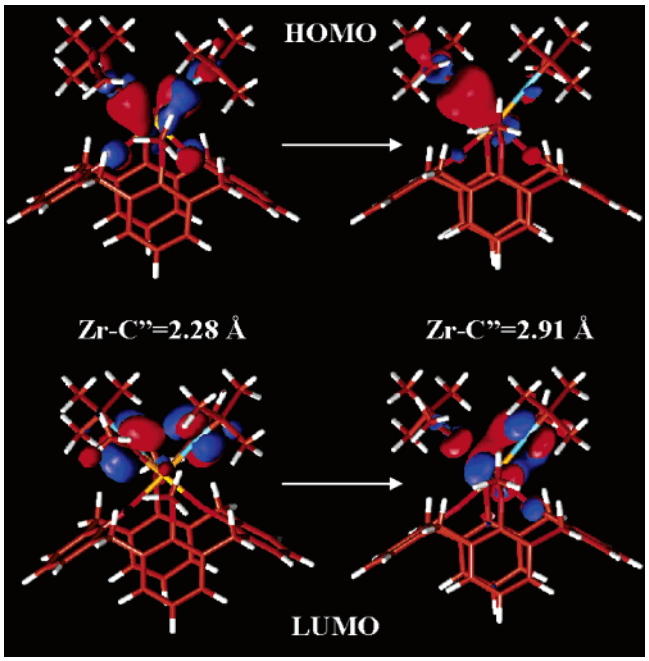

Figure 7. Isodensity surface plots of the HOMO and LUMO for the bis(η^2-iminoacyl) complex **1a** as a function of the Zr−C″ distance. The Zr−C″ value of 2.28 Å corresponds to the equilibrium value of this parameter in complex **1a**.

cupied molecular orbital (LUMO) is a combination of the two iminoacyl π^* orbitals, again symmetrically delocalized on the two iminoacyl units. Following the system evolution along the Zr−C″ approximate RC, we notice that for a value of the RC of 2.91 Å, corresponding to breaking of the Zr−C″ bond, a sizable change in the electronic structure takes place. In particular, the HOMO is now mainly composed by a lone pair of the decoordinated iminoacyl carbon, while the LUMO is an iminoacyl π^* combination localized essentially on the coordinated iminoacyl unit and on the metal (see Figure 7). This orbital picture suggests that the iminoacyl coupling process is initialized by the electronic structure change following the elongation of the Zr−C″ distance and can be therefore described as an intramolecular attack of the decoordinated iminoacyl carbon lone pair at the coordinated iminoacyl π^* orbital. This is confirmed by the fact that at the $\mathbf{TS_{1a\rightarrow 2a}}$ geometry, where the detached iminoacyl C″ (Zr−C″ = 2.934 Å) attacks the coordinated iminoacyl unit, the HOMO appears to be composed of a combination of the decoordinated iminoacyl carbon lone pair and of the coordinated iminoacyl π^* orbital (Supporting Information). This orbital evolution pattern is similar to the situation encountered in methyl to acyl and methyl to iminoacyl migrations in Zr−calix[4]arene systems.[32−34]

Conclusions

The intramolecular coupling of the two iminoacyl units in the bis(η^2-iminoacyl) complexes [calix[4](OMe)$_2$(O)$_2$−Zr(η^2-MeCNBu^t)$_2$] and [(2,6-Bu$^t_2$C$_6$H$_3$O)$_2$−Zr(η^2-MeCNPh)$_2$] to generate the corresponding enediamido species has been investigated by means of both static and dynamic density functional calculations. For both systems we have characterized the stationary points of the potential energy surfaces for the coupling reaction and evaluated the overall energy profile. Car−Parrinello molecular dynamics simulations have been performed to gain insight into the detailed mechanistic features of the iminoacyl coupling. Our results surprisingly show that this reaction occurs through an asynchronous mechanism in which a decoordinated iminoacyl carbon attacks the residual coordinated iminoacyl C−N double bond. A transition state search, performed

without any symmetry constraints, led to structures consistent with the proposed reaction mechanism, which were located 23.8 and 21.2 kcal mol^{-1} above the starting bis(η^2-iminoacyl) reagents, for the bis(aryloxide) and calix[4]arene species, respectively, in good agreement with experimental activation enthalpies. On the basis of the proposed reaction mechanism, we are also able to reproduce the activation energy of the coupling reaction with electron-withdrawing substituents on the iminoacyl moiety.

Inspection of the electronic structure changes along the proposed reaction mechanism reveals that the HOMO becomes essentially a carbon lone pair of the decoordinated iminoacyl unit, while the LUMO, of iminoacyl π^* character, becomes mainly localized on the coordinated iminoacyl unit and on the metal. This orbital evolution picture, together with the computed transition-state geometry, suggests that the iminoacyl coupling process can be described as an intramolecular attack of the decoordinated iminoacyl carbon lone pair at the coordinated iminoacyl π^* orbital, a situation similar to that encountered in methyl to acyl and methyl to iminoacyl migrations in Zr−calix[4]arene systems, thus reconciling the iminoacyl coupling reaction mechanism with the generally accepted pattern of acyl and iminoacyl reactivity.

Supporting Information Available: A movie file of the CP trajectory and a figure giving the isodensity surface plot of the HOMO at the $\mathbf{TS_{1a\rightarrow 2a}}$ geometry. This material is available free of charge via the Internet at http://www.pubs.acs.org.

OM0491591